Semi-automatic needle steering system with robotic manipulator

Mariana C. Bernardes, Bruno V. Adorno, Philippe Poignet, Geovany A. Borges

Abstract— This paper presents a semi-automatic system for robotically assisted 2D needle steering that uses duty-cycling to perform insertions with arcs of adjustable curvature radius. It combines image feedback manually provided by an operator with an adaptive path planning strategy to compensate for system uncertainties and changes in the workspace during the procedure. Experimental results are presented to validate the proposed platform.

I. INTRODUCTION

Special needles capable of active steering during their insertion have been designed to expand the applicability of percutaneous procedures [1]. These needles use their great flexibility and beveled tips to enhance and magnify the needle deflection effect, allowing curved trajectories that could be used to avoid sensitive or impenetrable areas inaccessible with conventional rigid needles.

When inserted into soft tissue, a steerable needle follows a curved path that is prescribed by the geometry of its beveled tip, its relative stiffness with respect to the tissue and the insertion and rotation velocities at the needle base. The curvature of the path can be adjusted during insertion using a duty-cycling technique [2] which combines simultaneous rotation and insertion movements of the needle.

In this kind of application, motion planning and control is a complex task and its difficulty increases as we consider the presence of uncertainties due to errors in tip positioning, needle modeling, tissue inhomogeneity, and deformation; thus the need of developing robotic steering systems capable of compensating for such effects.

In this paper, we present an adaptive approach for semi-automatic insertion of steerable needles using a robotic manipulator. It combines the Arc-based RRT path planner [3] with tip position feedback provided by an operator to compensate for system uncertainties and changes in the workspace or in the target position that may occur during the insertion procedure. Experimental results are shown to validate the proposed platform and confirm the advantage of using image feedback combined with an adaptive replanning strategy.

M.C. Bernardes and P. Poignet are with Université Montpellier 2, LIRMM, 161 rue Ada, 34095 Montpellier, France {bernardes,poignet}@lirmm.fr

B.V. Adorno is with Universidade Federal de Minas Gerais, Av. Antônio Carlos 6627, 31270-010 Belo Horizonte-MG, Brazil adorno@cpdee.ufmg.br

G.A. Borges and M.C. Bernardes are with Universidade de Brasília, LARA, Caixa Postal 4386, 70919-970 Brasília-DF, Brazil {gaborges,bernardes}@unb.br

A. Related work

The first types of robotically assisted systems for needle steering were dedicated devices that operated in open-loop from a sequence of previously assigned insertion and rotation movements [4]. The goal of these initial works was mainly to evaluate the bending effects of the interaction between needle and tissue. Online update of rotation and insertion velocity references was first introduced by Romano et al. [5]. They proposed a teleoperation system where the control inputs are provided by an operator with a haptic device.

Kallem and Cowan [6] developed an observer-based controller to drive the needle to a desired plane, and they concluded that the stabilization of the needle 2D working plane can improve the performance of 2D planners when used combined. This was shown in the article of Reed et al. [7], which presents a functional needle steering system that integrates patient-specific 2D pre- and intra-operative planning [8] together with Kallem and Cowan's image-guided feedback controller [6] and torsion compensation [9]. At the best of our knowledge, this was the first system to integrate planning and control for automatic online correction of the needle trajectory. However, their system requires a dedicated two-DOF device, and the use of intra-operative planning is suitable only for static workspaces, since it relies on a roadmap constructed pre-operatively.

More recent works also use robotically guided systems; for instance, Asadian et al. [10] used a robot with five DOF to evaluate a planning method based on offline optimization algorithms. The system is capable of compensating for uncertainties offline, but has no intraoperative adaptation, and hence is not suitable for dynamic workspaces.

Wood et al. [11] used a dedicated two-DOF device combined with image feedback to control the needle curvature. They used a duty-cycling strategy in order to track a trajectory provided pre-operatively. Because the system does not perform trajectory update, changes in the workspace are not taken into account in the needle insertion.

B. Contributions and organization of the paper

The main contribution of this work is the proposal of a robotically assisted system for 2D needle steering combined with image feedback. The method uses information from the current tip position to update the planned needle trajectory intraoperatively. Differently from previous approaches, this paper takes the dynamic nature of the workspace into account, so it can also compensate for changes in the obstacles and the target position.

The paper is organized as follows. Section II presents the kinematic model for steerable needles actuated by duty-
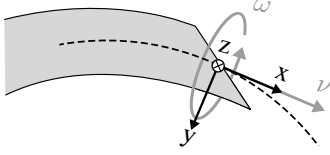
Fig. 1: Needle coordinate system and control inputs.

cycling. Then, a brief introduction about the proposed architecture is given in Section III. In the sequence, in Sections IV and V, the system modules are described in more detail. Section VI presents the experimental setup and obtained results. Finally, Section VII presents the conclusions and possible future work.

II. STEERABLE NEEDLE KINEMATIC MODEL

When pushed forward, the natural behavior of a steerable needle is to bend in the direction of its sharpened tip, following an arc of approximately constant curvature $\kappa_{\max}$, as illustrated in Fig. 1. The kinematic model for this kind of needle can be approximated by that of a nonholonomic unicycle vehicle [1], with the following nonholonomic constraints: $\omega_y = \nu_y = \nu_z = 0$ and $\omega_z = \nu_x \kappa_{\max}$. Thus, the system has two control inputs ν_x and ω_x, that are respectively the needle's insertion and rotation velocities along the x-axis, and are referred simply as ν and ω.

If simultaneous rotation and insertion velocities are combined, the needle moves along an helical path in the 3D space. In the case of using a rotation velocity substantially larger than the insertion velocity, the helix curvature tends to zero. Consequently, the needle follows a straight trajectory in its xy-plane. The duty-cycle technique explores such idea to achieve different curvature values.

This strategy combines periods T_{ins} of pure insertion with periods T_{rot} of simultaneous insertion and rotation, so that any curvature ranging from the natural curvature to a pure straight trajectory can be achieved. The duty-cycle DC is defined as the ratio of T_{rot} to the cycle period T:

$$DC = \frac{T_{\mathrm{rot}}}{T} = \frac{T_{\mathrm{rot}}}{T_{\mathrm{rot}} + T_{\mathrm{ins}}}. \tag{1}$$

There is a linear relationship between curvature and duty-cycle [12], so any path curvature in the range $[0, \kappa_{\max}]$ can be obtained by a proper choice of DC:

$$\kappa = \kappa_{\max}(1 - DC), \tag{2}$$

where κ is the effective curvature and $\kappa_{\max}$ is the needle natural curvature, when no spinning is applied.

We assume that the needle xy-plane is kept aligned to the desired 2D work plane during the insertion. Therefore, the rotation speed is chosen to be much higher than the insertion speed and the needle must perform complete rotations at each cycle. As a consequence, the rotation period is chosen to be $2\pi n\omega^{-1}$ with $n = 1, 2, 3, \ldots$ By making T_{rot} a fixed value, the insertion period T_{ins} must be adjusted in order to achieve a desired curvature. This method can be easily implemented by fixing the rotational speed $\omega = \omega_{\mathrm{ref}}$ and moving a fixed
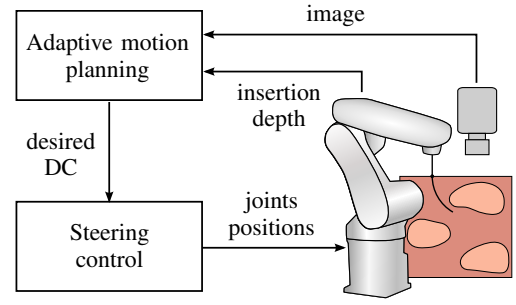

Fig. 2: Proposed system.

insertion distance $\triangle s$ at each cycle, so that the insertion velocity is variable and given by

$$\nu = \frac{\triangle s}{T}. \tag{3}$$

The coordination between rotation and insertion motion is performed by the *duty-cycle control*, described in Section V-A.

III. NEEDLE STEERING SYSTEM

The proposed needle steering system (see Fig. 2) can be separated in two main modules—the *adaptive motion planner* and the *steering controller*. The *adaptive motion planner* is responsible for calculating the desired trajectory for the needle insertion, while the *steering controller* applies the correspondent ω and ν inputs that will drive the needle through the planned trajectory. The description of each module is provided in the next sections.

IV. ADAPTIVE MOTION PLANNING

The *adaptive motion planning* module (see Fig. 3) calculates a trajectory for the needle tip and uses image feedback to update the planned path during the insertion procedure. To be able to adapt the trajectory online, the path planner has to be fast enough while respecting the workspace configuration and the needle's nonholonomic constraints. In this paper, we use an algorithm that we developed previously—the Arc-based RRT planner [3]—which uses explicit geometry to obtain feasible trajectories that respect the needle nonholonomic constraints. In this manner, the planner can be used intraoperatively thanks to its high success rate and fast calculation time.
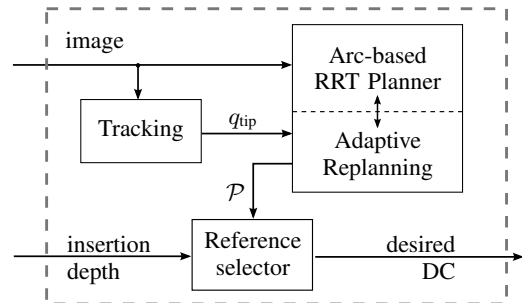

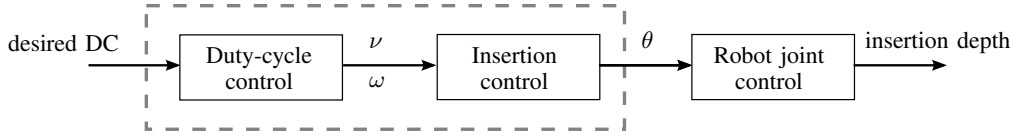Fig. 3: Module of the adaptive motion planning.

Fig. 4: Steering control module inside the dashed rectangle.

A. Image-based path planning

Let the configuration q of a needle to be defined by its tip cartesian coordinates $p = (x, y)^T$ and orientation angle φ in the working 2D plane. The objective of the Arc-based RRT planner is to find a combination of circular arcs capable of taking the needle from its initial configuration $q_{init} = (x_{init}, y_{init}, \varphi_{init})^T$ to a final position $p_{goal} = (x_{goal}, y_{goal})^T$ while avoiding obstacles present in the workspace and respecting the needle's nonholonomic constraints.

During the insertion procedure, the obtained path $\mathcal{P}$ is constantly updated by the Adaptive Replanning until the needle tip is sufficiently close to the target. The Adaptive Replanning uses the current needle tip configuration provided by the tracking module and the workspace obtained from camera images to adjust the path $\mathcal{P}$ when possible or to recalculate a new one if a collision is detected in the updated arcs, or if the new curvature does not respect the maximum limit κ_{max}. More details of the algorithm can be found in [3].

B. Needle tracking

The needle tracking is responsible for updating the current tip configuration q_{tip} to be used by the Adaptive Replanning. In our semi-automatic system, it consists of a user interface which should be used by the operator during the insertion procedure to correct the estimated tip position. This correction can be done at anytime with simple mouse clicks on the image. In an automatic system, this interface could be replaced by an image processing module with object tracking. Every time the current tip configuration is updated by the tracking module, the Adaptive Replanning algorithm is run to update the desired needle path.

C. Reference selection

The Reference selector receives the planned path $\mathcal{P}$ and calculates the correspondent duty-cycle sequence parametrized in insertion depth that will take the needle from its insertion point to the goal while following the desired path. This sequence is recomputed every time $\mathcal{P}$ is updated and it is obtained from the accumulated arcs lengths and from the linear relation between duty-cycle and desired arc curvature given by (2). The desired DC reference is then selected according to the current insertion depth and passed to the *steering control* module.

V. STEERING CONTROL

The *steering control* module (see Fig. 4) is responsible for actuating the manipulator while trying to assure that the needle will be kept in the desired 2D work plane. It consists mainly of two parts—the *duty-cycle control*, which coordinates the rotation and insertion movements by choosing
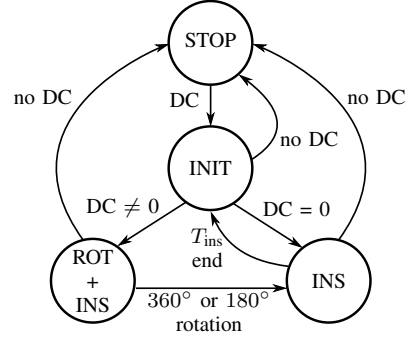

Fig. 5: Duty-cycle control state-machine.

appropriate reference values for ω and ν; and the *insertion control*, which computes the joints positions θ that will provide a purely vertical movement along the end-effector z-axis with the desired insertion velocity ν. The manipulator has six DOF, and the first five DOF are used by the *insertion control* while the sixth and last DOF is used in the *duty-cycle control*.

A. Duty-cycle control

The *duty-cycle control* actuates in the last joint of the manipulator which performs the rotation of the end-effector where the needle is attached. This controller has a state machine to alternate between $\omega = 0$ or $\omega = \omega_{ref}$ and calculates the periods T_{rot} and T_{ins} that will provide the desired DC received as reference. By choosing a fixed value for ω_{ref}, the rotation period T_{rot} is also constant and T_{ins} is obtained from (1). At last, the velocity insertion ν is computed from (3).

The implemented state machine is presented in Fig. 5 and it has the following states:
STOP: when there is no duty-cycle signal to be applied;
INIT: initializes a cycle and chooses between pure insertion or simultaneous rotation and insertion;
ROT + INS: applies simultaneous rotation and insertion. This state is kept until a half or full turn is performed depending on the desired arc direction;
INS: applies pure insertion. This state is kept until the expected insertion period ends.

The duty-cycle controller checks the last joint angle before entering in the insertion state to assure that a complete turn was performed in each cycle so that the needle is expected to stay in a nearly constant 2D plane. It is also responsible for reorienting the needle tip every time there is a curvature inversion. This controller actuates only in the manipulator's 6th DOF, leaving the other five DOF to the *insertion controller*.

B. Insertion control

The 3D configuration of the robot's end-effector can be described by a rigid transformation from the robot base frame O_{base} to its end-effector frame O_{effector} in dual quaternion representation [13]. The dual quaternion

$$\underline{\mathbf{q}} = \begin{bmatrix} \mathbf{q}^T & \frac{1}{2}(\mathbf{t}\mathbf{q})^T \end{bmatrix}^T \tag{4}$$

describing a rigid transformation is a dual entity composed of a unit quaternion $\mathbf{q}$ representing a rotation through the origin of O_{effector} and a quaternion $\mathbf{q}' = \frac{1}{2}\mathbf{t}\mathbf{q}$, indirectly representing a translation from the origin of O_{base} to O_{effector} .

The steerable needle is attached to the manipulator's end-effector so that the movements of the latter will be transmitted directly to the former. The objective of the *insertion controller* is to apply the translational velocity ν provided by the *duty-cycle control*, while conserving the end-effector's horizontal position and vertical orientation, and thus, constraining it to translate only in a vertical fashion.

The controlled variables are represented by the vector

$$\mathbf{x} = \begin{bmatrix} \beta & x & y & \nu \end{bmatrix}^T,$$

where β is the angle between the z-axis of O_{effector} and the z-axis of O_{base}, x and y are the end-effector's position coordinates, and ν is the insertion velocity given in the z-axis direction of O_{effector} (see Fig. 6). To assure a vertical insertion, we want β to be always zero, and x and y to correspond to their initial values.

If we define θ_k as the robot's joints positions in time step $k = 0, 1, 2, \ldots$, the control input is given by the discrete PID controller:

$$\theta_k = \theta_{k-1} + J_k \left[K_p \mathbf{e}_k + K_i \sum_{i=1}^{k} \mathbf{e}_i + K_d(\mathbf{e}_k - \mathbf{e}_{k-1}) \right],$$

where $\mathbf{e}_k = \mathbf{x}_{\text{des}_k} - \mathbf{x}_k$, in which $\mathbf{x}_{\text{des}_k}$ and $\mathbf{x}_k$ are the desired and measured values of the control variables, respectively.

J_k is the Jacobian that satisfies $\dot{\mathbf{x}}_k = J_k \dot{\theta}_k$ and can be divided in two parts:

$$J_k = \begin{bmatrix} J_\beta^T & J_\nu^T \end{bmatrix}^T.$$

The angle β is obtained from the current end-effector's configuration $\underline{\mathbf{q}}_k$:

$$\beta = \arcsin(2q_1 q_2 - 2q_4 q_2), \tag{5}$$

with q_i representing the i-th term of vector $\underline{\mathbf{q}}_k$. Derivating (5), we have that $\dot{\beta} = J_\beta \dot{\theta}$, with J_β given by

$$J_\beta = \frac{2}{\sqrt{1 - 4(q_1 q_3 + q_4 q_2)^2}} \begin{bmatrix} q_3 & -q_4 & q_1 & -q_2 \end{bmatrix} J_{\mathbf{q}'}.$$

From the robot's Denavit-Hartenberg model, it is possible to obtain both J_g and $J_{\mathbf{q}}$ which are, respectively, the geometric and the analytic Jacobians [13]. J_ν is the part of the geometric Jacobian for the translational velocities, while $J_{\mathbf{q}'}$ is the dual part of the analytic Jacobian:

$$J_g = \begin{bmatrix} J_\nu^T & J_\omega^T \end{bmatrix}^T \qquad J_{\underline{\mathbf{q}}} = \begin{bmatrix} J_{\mathbf{q}}^T & J_{\mathbf{q}'}^T \end{bmatrix}^T.$$
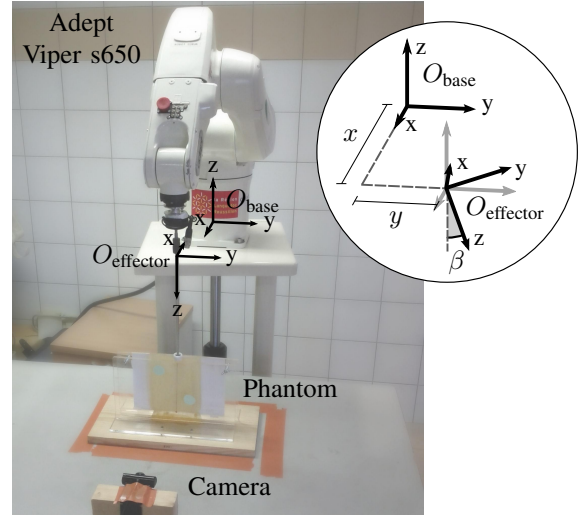

Fig. 6: Experimental setup with the Adept Viper s650. The *insertion controller* variables are shown in detail.

VI. Experiments

A. Experimental setup

The *adaptive motion planner* and *steering control* modules were divided into two different computers which communicate by TCP protocol. The *adaptive motion planner* executes in a PC with Linux operating system and equipped with a HD 720p webcam (4.21 mm focal length and 1280x720 video resolution). The *steering control* module is run in a PC with Linux RTAI and connected by firewire communication to an Adept Viper s650. The needle prototype consists of a 0.8 mm diameter nitinol wire with approximately $16°$ bevel tip angle. The phantom was made of plastisol—a suspension of PVC particles in plasticizer (Plastileurre® Rigide, Bricoleurre SARL).

The end-effector of the Viper robot has a gripper in which the base of the needle is attached and where a telescopic tube is placed to prevent the needle from buckling. Below the end-effector, an acrylic support with the semi-transparent plastic phantom is placed to receive the needle. The webcam is positioned in front of the phantom to register the progress of the insertion and also to give visual feedback to the operator. The experimental setup is shown in Fig. 6.

After the needle is attached to the robot, a calibration process is performed to assure that the bevel of the needle is pointing to the plane of the plastic phantom. The calibration consists in doing several insertions with 0% duty-cycle—that is, pure insertion—and adjusting the needle orientation up to a few degrees until it can be completely inserted without going out of the plane more than a few millimeters.

In addition, the camera must be calibrated to assure that the image plane corresponds to the same plane of the acrylic support. For this, a chess pattern with squares of known size is temporarily fixed in the acrylic plane. The corners of the pattern are extracted and used to build a Metric Rectification Homography matrix [14] which is stored and used to rectify the images during the experiments. The chess pattern is also

used to extract the image resolution [m/pixel] by applying a least-square minimization. The obtained resolution value is used by the *adaptive motion planner* to convert the insertion depth information from meters to image pixels.

At last, the natural curvature $\kappa_{\max}$ for the needle-tissue combination should be identified. For this, a series of pure insertions is performed and the images of each procedure are stored and evaluated offline. For each insertion, a curve fitting optimization is done using the `nlinfit` command from Matlab. This function implements a non-linear least-square method that uses Gauss-Newton descent algorithm with Levenberg-Marquardt modifications for global convergence. The final estimated natural curvature is given by the mean of the obtained values.

Every experiment has an initialization step in which the operator selects in the webcam image the desired workspace region, the obstacles, the needle's initial entry point and angle, and the desired target. After this step, the Arc-based RRT planner calculates the needle path and the insertion procedure begins. At any point during the insertion, the operator may click on the images to update the actual needle configuration and, consequently, provide the image feedback used by the Adaptive Replanning to correct the desired trajectory and duty-cycle references.

B. Results

In this paper, the combination of phantom and needle available for the experiments provided very low steerability. The minimum curvature radius obtained from the offline identification procedure was approximately 25 cm while the values presented in the literature normally vary between 10 cm to 6 cm. As a result, the system actuation was easily saturated and the experimental scenarios for the needle insertion had to be restricted to single arc paths.

Two experiments were made with the proposed experimental platform. In the first experiment, the insertion was performed without updating the current needle configuration, so no feedback was provided to the Adaptive Replanning and, consequently, no correction was performed during the whole experiment. This open-loop procedure resulted in a final positioning error of approximately 13.7 mm and is shown in Fig. 7(a).

A second insertion was made, this time with an operator providing occasional updates in the tip configuration whenever he judged the needle was deviating from the expected path. The updates were done by performing clicks in the image to give the current tip position and orientation. Then, the desired needle path was automatically updated and the corresponding duty-cycle control input was automatically corrected. This is illustrated in Figs. 8 and 9, where operator's inputs resulted in changes in the planned path and in the desired DC. The final tip positioning for this second experiment had a final error of approximately 2.8 mm, and is shown in Fig. 7(b).

We observed that even very few updates in the current tip configuration were enough to provide a better performance of the procedure because they compensated for uncertainties

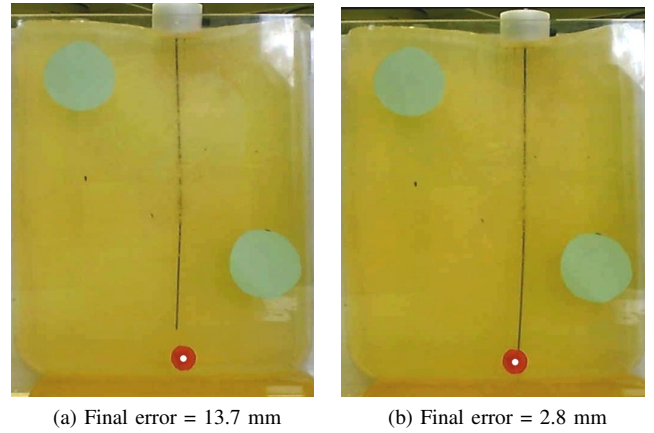(a) Final error = 13.7 mm   (b) Final error = 2.8 mm

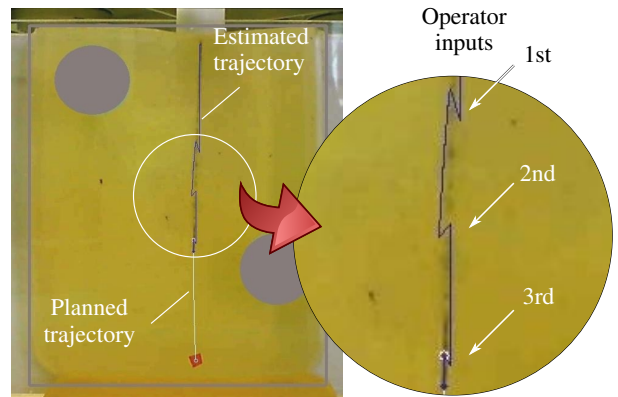Fig. 7: Needle tip final positions (a) in open-loop experiment and (b) with the Adaptive Replanning.

Fig. 8: Operator inputs update the expected trajectory.

such as modeling errors and uncertainties in the initial tip positioning and orientation. We may expect that the replacement of the manual update of the needle position by a continuous and automatic feedback provided by an image processing module with object tracking will result in a much better performance of the Adaptive Replanning.

The *steering control* also has shown to work properly. The proposed state machine was able to perform the needle duty-cycling as shown in Fig. 9. In this figure, one can observe that larger values of the duty-cycle correspond to bigger proportions of time during which the angular velocity is different from zero, as described in (1). The *insertion control* also presented a good performance, with position errors of less then 1 mm, orientation error lower then 1 degree and velocity errors in the order of 0.5 mm/s (see Fig. 10).

VII. CONCLUSION

In this paper we proposed an adaptive system for semi-automatic needle steering that uses a path planning approach that we had previously developed [3]. The use of image feedback combined with an adaptive replanning strategy improved the precision of the insertion procedure even with few updates provided by the operator.
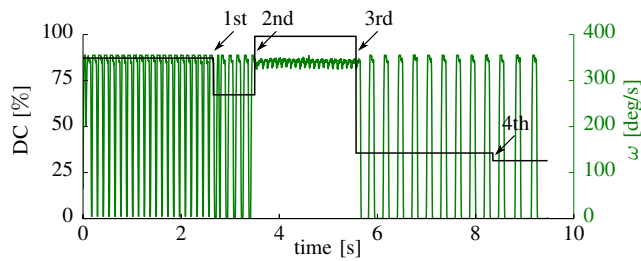
Fig. 9: Desired DC reference and correspondent ω output provided by the *duty-cycle control*. The arrows indicate the instants when the operator provided feedback.

Fig. 10: Error values of the *insertion control* states.

The presented results have been able to validate the platform and the control architecture, but we expect to explore more possibilities in future experiments with a needle-tissue combination that allows more sophisticated trajectories and online obstacle avoidance, which is previewed by our Arc-based RRT and the Adaptive Replanning approach. Also, it has been observed that the manual selection of the needle orientation is not very precise and adds additional errors to the system. We expect that the replacement of the manual feedback for an automatic object tracking system, which is currently under development, will provide even better results.

One of the main concerns for the *duty-cycle control* was to assure that the needle was kept in the same 2D plane during the insertion. For this, it was very important that the needle tip performed a complete revolution at each cycle. In the experimental trials, we observed that the needle stayed in the desired 2D plane. This evidence indicates that the continuous rotation in the same direction provided by the duty-cycling technique may decrease the effect of the torsional stiffness and allow a better transmission of the rotation movement to the needle tip. However, this behavior has to be further investigated and even if verified, it does not preclude the use of a low-level controller for plane stabilization as the one proposed in [6], since there is still need to compensate for errors in the needle's initial orientation.

There is a possibility of increased tissue damage resulting from the rotation of beveled tip needles and this is an important concern for clinical use of the duty-cycling technique. Podder et al. [15] investigated the effects of bevel tip needle rotation in plastic phantoms and did not observe significant enhance of damage. However, other articles have raised concerns about soft tissue injure. Although they conclude this should not prohibit the use of rotation as long as its effects are considered in risk analysis [16], future research should investigate safe velocity limits and needle design to minimize potential damage.

ACKNOWLEDGMENTS

REFERENCES

[1] R. Webster III, J. Kim, N. Cowan, G. Chirikjian, and A. Okamura, "Nonholonomic modeling of needle steering," *The Int. Journal of Robotics Research*, vol. 25, no. 5-6, pp. 509–525, 2006.
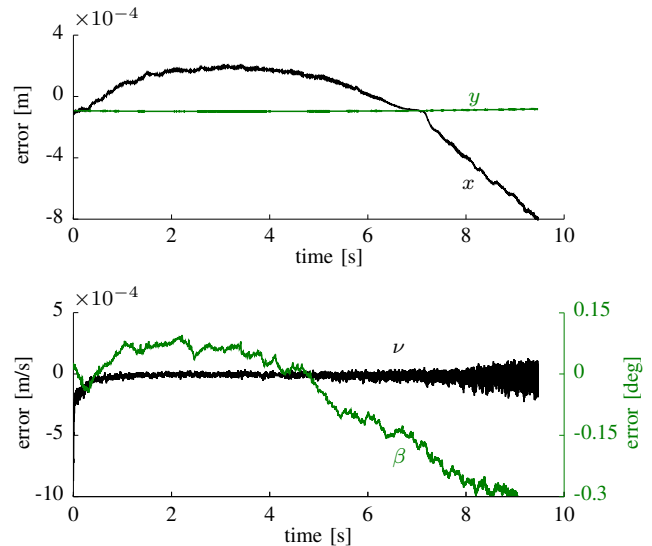
[2] J. Engh, G. Podnar, S. Khoo, and C. Riviere, "Flexible Needle Steering System for Percutaneous Access to Deep Zones of the Brain," in *Proc. IEEE Annual Northeast Bioengineering Conf.*, 2006, pp. 103–104.

[3] M. C. Bernardes, B. V. Adorno, P. Poignet, N. Zemiti, and G. A. Borges, "Adaptive path planning for steerable needles using duty-cycling," in *Proc. IEEE Int. Conf. on Intelligent Robots and Systems*, 2011, pp. 2545–2550.

[4] R. J. Webster III, J. Memisevic, and A. M. Okamura, "Design considerations for robotic needle steering," in *Proc. IEEE Int. Conf. on Robotics and Automation*, 2005, pp. 3588–3594.

[5] J. M. Romano, R. J. Webster III, and A. M. Okamura, "Teleoperation of Steerable Needles," in *Proc. IEEE Int. Conf. on Robotics and Automation*, 2007, pp. 934–939.

[6] V. Kallem and N. Cowan, "Image Guidance of Flexible Tip-Steerable Needles," *IEEE Trans. on Robotics*, vol. 25, no. 1, pp. 191–196, 2009.

[7] K. B. Reed, V. Kallem, R. Alterovitz, K. Y. Goldberg, A. M. Okamura, and N. J. Cowan, "Integrated Planning and Image-Guided Control for Planar Needle Steering," in *Proc. IEEE/RAS-EMBS Int. Conf. on Biomedical Robotics and Biomechatronics*, 2008, pp. 819–824.

[8] R. Alterovitz and K. Goldberg, "The Stochastic Motion Roadmap: A Sampling Framework for Planning with Markov Motion Uncertainty," *Robotics: Science and Systems*, 2007.

[9] K. B. Reed, A. M. Okamura, and N. J. Cowan, "Modeling and control of needles with torsional friction," *IEEE Trans. on Biomedical Engineering*, vol. 56, no. 12, pp. 2905–16, 2009.

[10] A. Asadian, M. R. Kermani, and R. V. Patel, "Robot-Assisted Needle Steering Using a Control Theoretic Approach," *Journal of Intelligent & Robotic Systems*, 2010.

[11] N. A. Wood, K. Shahrour, M. C. Ost, and C. N. Riviere, "Needle Steering System using Duty-Cycled Rotation for Percutaneous Kidney Access," in *Proc. IEEE Annual Int. Conf. of the EMBS*, 2010, pp. 5432–5435.

[12] D. Minhas, J. Engh, M. Fenske, and C. Riviere, "Modeling of needle steering via duty-cycled spinning," in *Proc. Annual Int. Conf. of the IEEE Eng. in Medicine and Biology Society*, 2007, pp. 2756–2759.

[13] B. V. Adorno, "Two-arm Manipulation: From Manipulators to Enhanced Human-Robot Collaboration," PhD Thesis, Université Montpellier 2, France, 2011.

[14] D. Liebowitz and A. Zisserman, "Metric rectification for perspective images of planes," in *Proc IEEE Computer Society Conf. on Computer Vision and Pattern Recognition*, 1998, pp. 482–488.

[15] T. K. Podder, D. P. Clark, J. Sherman, D. Fuller, E. M. Messing, D. J. Rubens, J. G. Strang, Y. D. Zhang, W. S. Ng, and Y. Yu, "Effects of tip geometry of surgical needles: an assessment of force and deflection," in *European Medical and Biological Eng. Conf.*, vol. 11, no. 1, 2005, pp. 5–8.

[16] S. Badaan, D. Petrisor, C. Kim, P. Mozer, D. Mazilu, L. Gruionu, A. Patriciu, K. Cleary, and D. Stoianovici, "Does needle rotation improve lesion targeting?" *Int J Med Robotics Assis Surg*, 2011.